Experimental and numerical study of water spray system for a fire event in a confined and mechanically ventilated compartment

Samuel Vaux, Hugues Prétrel, Laurent Audouin

Received: 16 April 2018 | Revised: 27 February 2019 | Accepted: 8 April 2019
DOI: 10.1002/fam.2719

WILEY

SPECIAL ISSUE PAPER

Experimental and numerical study of water spray system for a fire event in a confined and mechanically ventilated compartment

Samuel Vaux | Hugues Prétrel | Laurent Audouin

PSN-RES, SA2I, BP 3, Institut de Radioprotection et de Sûreté Nucléaire (IRSN), St Paul-Lez-Durance Cedex, France

Correspondence
Samuel Vaux, PSN-RES, SA2I, BP 3, 13115, Institut de Radioprotection et de Sûreté Nucléaire (IRSN), St Paul-Lez-Durance Cedex, France.
Email: samuel.vaux@irsn.fr

Summary

The present work addresses the application of a water spray system in case of a fire event in large-scale experiments for nuclear safety issues. It focuses on the interaction between a water spray system and a stratified smoke layer due to a pool fire in a mechanically ventilated enclosure. This study is supported by a set of four large-scale tests and one numerical simulation with a 3D CFD software, named CALIF^{3}S/ISIS, and developed by the French Institut de Radioprotection et de Sûreté Nucléaire (IRSN). The modelling used in this paper is based on an Eulerian-Lagrangian approach. The fire tests are performed in a 165 – m^3 mechanically ventilated single room. The fire is a lubricant oil pool fire of about 400 kW. The ventilation flow rate is 2550 $m^3.h^{-1}$ and corresponds to a renewal rate of 15.5 h^{-1}. The spray nozzles are deluge and sprinkler type. The test parameters are the water flow rate, the time of activation, and the duration of activation. Based on the large-scale experiments and the numerical simulation, four typical physical mechanisms have been enlightened. The first one corresponds to the cooling of the gas phase that is the straightforward consequence of the heat transfer exchange between the water droplets and the surrounding gas. The second effect is the process of gas mixing and homogenization induced by the water spraying system. The gas concentrations (O_2, CO_2) in the upper and lower parts of the room tend to the same level. The third effect is the significant increase of the fire heat release rate (HRR), up to 25 %, when the water spray is activated. Then, the last noteworthy effect is the occurrence of gas pressure peaks when the water spray is activated or shut off, consequence of the sudden change of the gas temperature. The processes of gas cooling and fire HRR increase are showed to be the main causes of these variations of gas pressure.

KEYWORDS
compartment, fire, mechanical ventilation, water spray system

1 | INTRODUCTION

In addition to the social and economic issues caused by the damage of a fire, research on spraying systems for fire safety applications remains significant because of the complexity of the interaction between water droplet media and fire environment. There is a continuous research activity to assess the performance of this fire protection system, to improve the prediction capability of the numerical tools (both zone and computational fluid dynamics [CFD] models[1]). and to develop efficient water spray systems for fire suppression, fire control, or smoke cooling. Two main issues are identified: the interactions between the droplets and the flame, with the final goal of fire suppression, and between the droplets and the smoke layer, for controlling the fire development. This study addresses the second issue in the specific environment of confined and mechanically ventilated enclosures. In that configuration, without the activation of a water spray system, the fire development often differs from that expected in an open atmosphere environment (eg, the effect of oxygen depletion on the fire source). When a water spray system is activated, additional specific phenomena occur including the pressure variation induced by the water spray, the smoke cooling efficiency, the process of thermal destratification of the smoke layer, and the amount of water vapor produced.

The occurrence of pressure variations is typical of a fire event in confined enclosures.[2] In case of activation of a water spray system, additional variations of pressure occur because of the sudden cooling of the gas phase. This phenomenon has been recently underlined by[3] mentioning low pressure peaks up to −10 hPa.

Other significant consequences are the phenomenon of smoke cooling and the modification of the smoke layer stratification. In a confined fire scenario, a noticeable effect of the activation of water spraying system is the downward displacement of the smoke layer leading to a change of the gas stratification and thus to a reduction of the visibility. In that case, although the water spray has a positive impact on the control of the fire, it may degrade the human evacuation efficiency. Several analytical approaches have been proposed to assess the downward displacement of the smoke layer as well as the heat transferred from the smoke to the droplet flow.[4-9] Some studies also point out this influence on the doorway flow or the vent flow.[10-12]

Very few studies on forced-ventilated compartment configurations have been performed in the scientific community. Recently, an experimental study[3] based on propane gas fire in the framework of the OECD PRISME2 project has discussed the interaction between droplets and the smoke as well as the droplet evaporation rate and the energy transfer from the dispersed phase to the continuous phase. The present contribution proposes to extend this previous fire scenario using a gas burner supplied with propane to an heptane pool fire. Four large-scale experiments are presented and a special emphasis on the effect of the water spray activation on the mass loss rate (MLR) of the pool is made. In addition, one CFD simulation is achieved on one scenario to test its ability to simulate relevant physical quantities such as the thermodynamic pressure, the thermal field, the species concentrations, and the ventilation flow rates.

The paper is organized as follows: in Section 2, the set of four experiments with an heptane pool fire is presented along with the water spray system; in Section 3, the main physical phenomena observed from the experiments are highlighted; in Section 4, the CFD simulation with the software CALIF^{3}S/ISIS is detailed and the results are discussed in Section 5. Finally, the main conclusions are drawn in Section 6.

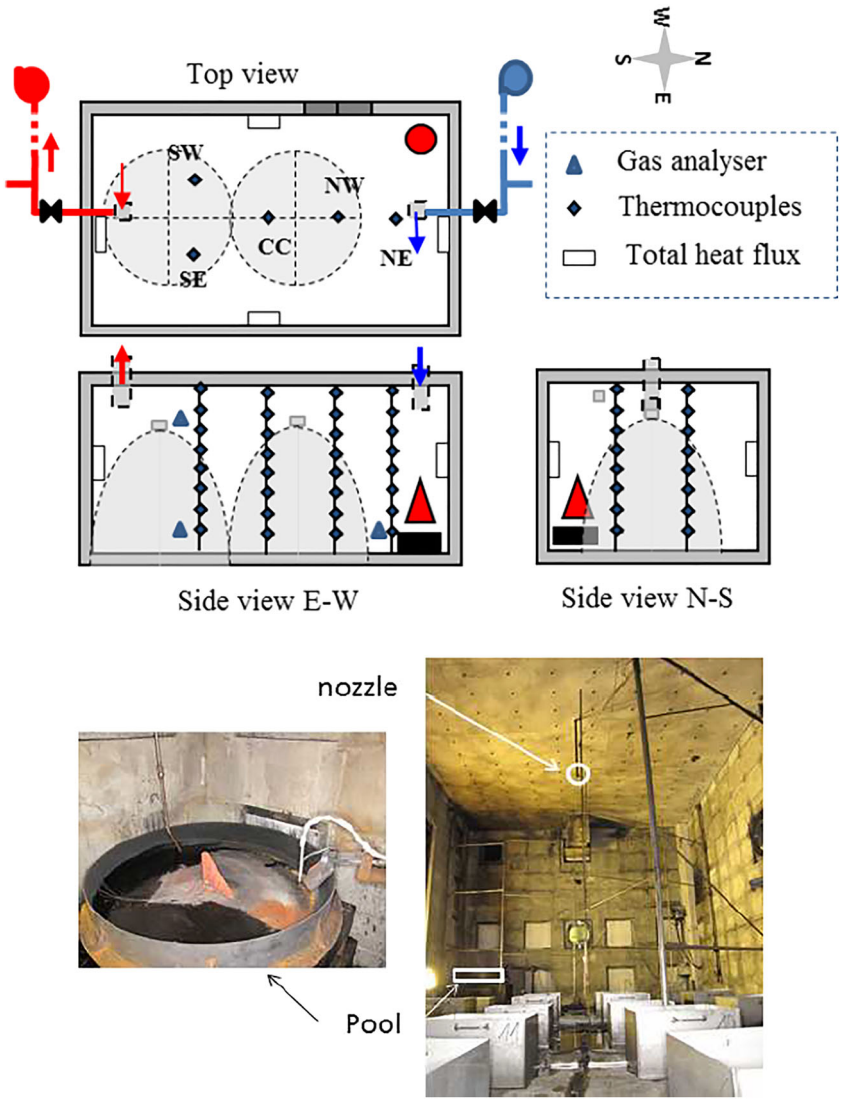

FIGURE 1 Sketch of the facility with the locations of the measurement points, the fire place, and the spray pattern [Colour figure can be viewed at wileyonlinelibrary.com]

2 | FIRE EXPERIMENTS

2.1 | Test configuration

The fire scenario, also presented in Pretrel,[3] consists in a fire in a confined and mechanically ventilated compartment. The compartment is a room of the IRSN DIVA facility, rectangular (4.88 m × 8.67 m = 42.3 m^2) with a height of 3.90 m (Figure 1). The walls, the floor, and the ceiling are made of concrete material, the ceiling being covered with silicate of calcium panels to avoid its thermal degradation. The ventilation system is composed of admission and exhaust lines connected to the room in the upper part at about 0.80 m from the ceiling. The ventilation lines are connected to an industrial network equipped with blowing and exhaust fans.

2.2 | Fire source

Whereas the fire source was a propane gas burner in the previous studies,[3] a liquid fuel pool fire is used in the present study. This fuel is lubricant oil (DTE Medium from Mobil), preheated before ignition and poured in the pan. The fuel properties are given in Table 1. The pool is a circular 0.7 m^2 pan, made of carbon steel with a depth of 130 mm. The pan is placed on a weighting device. The fuel is poured into the tank through a fixed metallic pipe coming from the preheater system. The mass of fuel is about 25 kg before ignition. The pool fire is ignited by a 20 − kW propane gas burner. The fire is located on the north-west corner of the room in order to avoid fire suppression due to water droplets and to study the interaction of the water spray with the hot smoke layer (cf. Figure 1).

2.3 | Water spray system

The water spray system is presented with details in Pretrel.[3] It is made of two nozzles located at 2.97 m from the ground and about 0.85 m from the ceiling (Figure 1). The nozzles are connected to a system of water pipes equipped with valves, a pressure transducer, and a water flow rate device. The water spray is activated and shut off manually using a valve on the water pipe system. Two nozzle types are considered, deluge and sprinkler, as illustrated in Figure 2. The deluge type is a Protectospray D3 high velocity nozzle with a K-factor of 26 l/min/bar$^{0.5}$. The sprinkler type is a Tyco TYB serie with a K-factor of 37 $l/min/bar^{0.5}$ from which the glass bulb was removed in order to activate the water spraying manually.

TABLE 1 Fuel properties

Name	DTE Medium Oil
Chemical composition	$C_{31}H_{64}$
Boiling point (°C)	480
Molar mass (g/mol)	440
Flash point (°C)	[195-270]
PCI (MJ/kg)	42.7
Density at 20 °C (g/ml)	0.870

2.4 | Measurements

The fuel mass is measured with a SARTORIUS weighting balance accurate to within 2 g. The fuel MLR is then determined from the time derivative of the mass. The ventilation flow rate is measured with averaging pitot tube devices, connected to pressure transducers and located in the inlet and exhaust ventilation ducts. The gas pressures in the room and in the ventilation network are also measured with pressure transducers.

The gas temperatures are measured with 1.5 mm K-type thermocouples fixed on five vertical masts (Figure 1) named SW, SE, CC, NE, and NW. The thermocouples are equipped with metal protective caps to prevent droplets coming into contact with their tips. Each mast is equipped with eight K-type thermocouples located at 0.55 m, 1.05 m, 1.55 m, 2.05 m, 2.55 m, 3.05 m, 3.55 m, and 3.90 m from the ground.

Oxygen and carbon dioxide concentrations are measured at three positions within the room: two on the SE mast, one at a lower position and the other in an upper position, and one close to the fire as well as in the ventilation ducts. Each sample point is connected to sampling system and gas analyzers for oxygen and carbon dioxide. Molar fractions are measured with a SERVOMEX XANTRA 4100 or EMERSON Xstream for oxygen and a SIEMENS ULTRAMAT 22-23 or EMERSON Xstream for carbon dioxide. The sampling system controls the pressure, the flow rate, and dries and filters the gas sample from soot. The molar fractions, presented here, are based on the dry sample. The time delay due to the sampling process is corrected. Measurement uncertainties are given in Pretrel and Querre.[13] In addition, Pretrel and Querre[13] also discuss the measurement variability due to repeatability. The PR2_FES_1 test was reproduced twice during the fire test campaign. The results indicate that oxygen concentrations and gas temperatures are the most reliable variables whereas the characteristics of the water spray (flow rate, density) and the characteristics in the ventilation (pressure and flowrate) are less repeatable.

2.5 | Test matrix and experimental procedure

A set of four tests have been performed in the fire extinction system (FES) campaign of the OECD PRISME2 project. For all tests, the fire scenario is identical and consists in a 0.7 m^2 oil pool fire located in

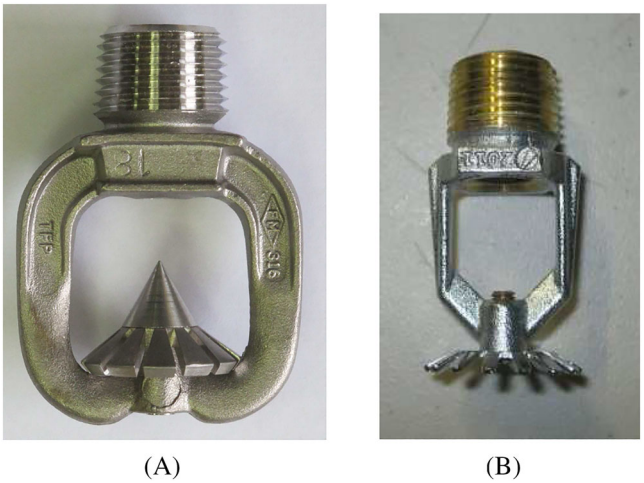

(A) (B)

FIGURE 2 Picture of A, a deluge nozzle and B, a sprinkler nozzle [Colour figure can be viewed at wileyonlinelibrary.com]

TABLE 2 Operating conditions of the water spray system (targeted values)

Test Name	PR2_FES_1	PR2_FES_2	PR2_FES_3	PR2_FES_4
Nozzle	Deluge	Deluge	Sprinkler	Sprinkler
Operating pressure (kPa)	450	450	222	450
Total flow rate (l/min)	110	110	110	157
Activation time	t_a = 948 s	$t_{80°C}$	$t_{80°C}$	$t_{80°C}$

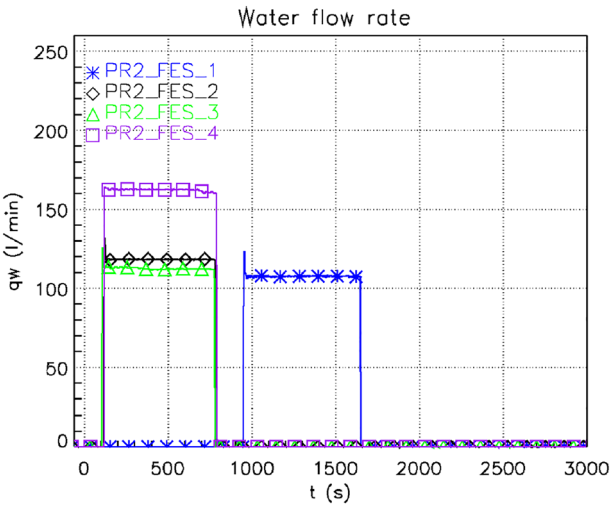

FIGURE 3 Time evolution of the total water flow rate delivered by the water spraying system [Colour figure can be viewed at wileyonlinelibrary.com]

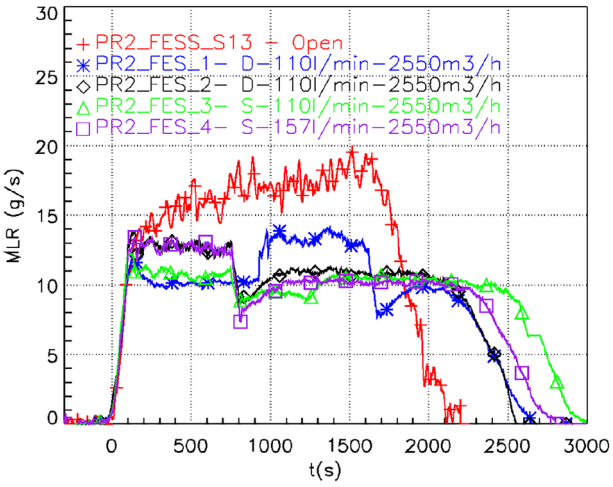

FIGURE 4 Time evolution of the fuel mass loss rate for the four tests and for the same fire source in open atmosphere [Colour figure can be viewed at wileyonlinelibrary.com]

a 165 − m^3 compartment mechanically ventilated at 2550 m^3/h and equipped with two water spray nozzles. The varying parameters are the type of nozzle (deluge or sprinkler), the total water flow rate (110 and 157 l/min), and the time at which the water spray is activated (see Table 2). The objective of the PR2_FES_1 test is twice. First, it aims at characterizing the behaviour of the fire source in a confined and ventilated environment without water spray system during the first stage of the test. Then, as soon as the fire source has reached a steady state, it focuses on the interaction between the hot smoke layer and the water droplets released by the activation of a spraying system. The objective of the PR2_FES_2 test is to study the effect of the activation time with the same nozzle, operating pressure, and water flow rate. The spray system was activated as soon as the gas temperature near the spray nozzles reached 80 °C (about 110 seconds after ignition). The PR2_FES_3 test is focused on the effect of the type of nozzle keeping constant the total water flow rate. The objective of the PR2_FES_4 test is to investigate the effect of water flow rate (increased to 157 l/min) for a given type of nozzle.

The test procedure was as follows. First, the targeted ventilation flow rate is stabilized by operating the ventilation network. Then, the fuel is poured in the pan and is ignited. The water spraying system was turned on 948 seconds after ignition for PR2_FES_1 test and 115,103, and 118 seconds for the three other tests, ie, PR2_FES_2, PR2_FES_3, and PR2_FES_4, respectively. The spraying period is similar for all tests and equal about to 10 minutes. The time variations of the total water flow rate for the four tests are presented in Figure 3.

3 | ANALYSIS OF THE FIRE TESTS

The analysis points out four particular physical behaviours directly related to the interaction between the fire source and the water spray in a confined and forced ventilated compartment. These items are the influence of the environment on the MLR, the pressure variation, the cooling, and the mixing of the gas phase.

3.1 | Influence of the environment on the MLR

The time variation of the MLR, represented in Figure 4, shows a typical behaviour for all the tests with a first period of fire growth, a period of steady combustion during which the water spray system is activated and a decay before extinction due to a lack of fuel in the pan. The MLRs are compared with the one measured in open atmosphere (Fire test PR2_FESS_S13 performed in the hood of IRSN). As expected, the average MLR during the steady period (10.5 g/s) is lower than the level achieved in open atmosphere (17.1 g/s). This result is typical of compartment fires when the oxygen concentration is lower than the value of 21% available in open atmosphere. Nevertheless, an unexpected increase of the MLR is clearly observed because of the effect of spray activation. To our knowledge, no clear explanation has yet been found for this phenomenon. A first hypothesis is to consider that the level of flow turbulence induced by the motion of the spray droplets is enhanced, which favors the availability of oxygen near the fire.[14] A second hypothesis lies in the observation of increased fuel MLR when water vapor is added to the fuel.[15] For the tests PR2_FES_1 and PR2_FES_2, the mean MLR increases from 10.5 g/s to 13 g/s. The change of the spray activation time does not affect this influence of the spray on the MLR (comparison between

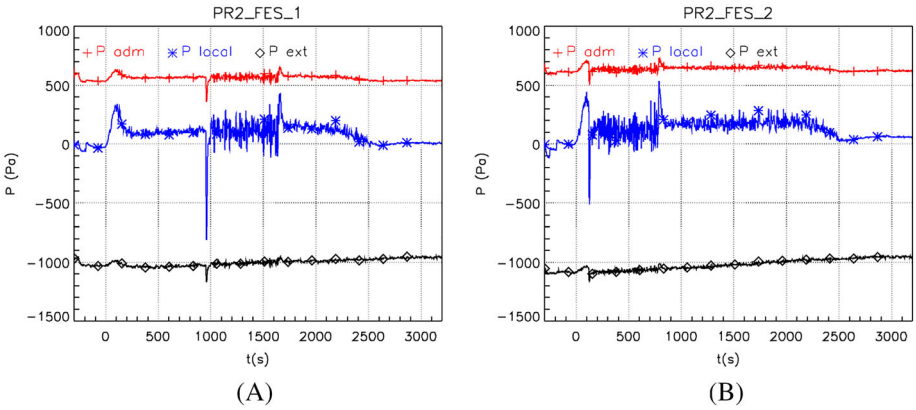

FIGURE 5 Time evolution of the pressure in the admission line, in the enclosure, and in the exhaust line for A, the PR2_FES_1 test and B, the PR2_FES_2 test [Colour figure can be viewed at wileyonlinelibrary.com]

tests PR2_FES_1 and PR2_FES_2) whereas the change of nozzle type (deluge for the PR2_FES_2 test and sprinkler for the PR2_FES_3 test) or in the water flow rate (sprinkler with 110 *l*/*min* for the PR2_FES_3 test and 157 *l*/*min* for the PR2_FES_4 test) do. The activation of the water spray system, if it does not succeed in extinguishing the fire source, may contribute to enhance the MLR. The water flow rate and the type of nozzle are parameters that may modulate this effect.

3.2 | Effect on the room pressure

The second noticeable effect is the variation of pressure that is a typical phenomenon observed for fire scenarios in confined and ventilated enclosures. For the present set of tests with the activation of water spraying systems, additional pressure variations are observed. Time variations of the static pressures measured in the fire room and in the ventilation lines (upstream and downstream the room) are presented in Figure 5 for tests PR2_FES_1 and PR2_FES_2. Typical over-pressure and low-pressure peaks are, respectively, noticed straight after ignition and extinction. Straight after ignition, the over-pressure peak is induced by the gas expansion due to the temperature increase. At extinction, the low-pressure peak, which is weak for these tests, results from temperature decrease. In addition, the activation and the shut off of water spraying also induce significant pressure variations. The first pressure peak at the water spray activation consists in a low-pressure variation resulting from the combination of two effects: the cooling of the gas phase by the water droplets and the increase of the fuel MLR. The two effects could induce opposite actions on the room pressure. The cooling contributes to a reduction of the room pressure whereas the MLR increase leads to an increase of the room pressure. For these tests, given that the net result is a pressure decrease (with the occurrence of a low-pressure peak), the cooling process appears to be the dominant effect. For the tests with an earlier activation (PR2_FES_2, PR2_FES_3 and PR2_FES_4 tests), the low-pressure peak occurs during the typical over-pressure of the fire growth period. The second peak, observed when the water spray is shut off, consists in an over-pressure. As for the first peak, it results also from two opposite effects: the stop of the gas cooling (the gas warms up again since the fuel still burns) and the reduction of the fuel MLR. Given that the net result is a pressure increase (with the occurrence of an over-pressure peak), the warming process appears

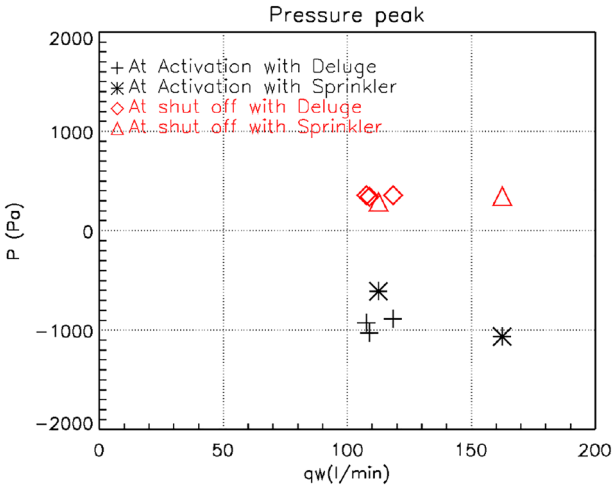

FIGURE 6 Variation of the pressure peaks versus the water flow rate for two instants (activation and shut-off) and for the two nozzles [Colour figure can be viewed at wileyonlinelibrary.com]

to be the dominant effect. The influence of the water flow rate and the type of nozzle on the pressure peaks is presented in Figure 6. The magnitude of the low-pressure peak when the water spray is activated increases with the water flow rate and is larger for the deluge nozzle than with the sprinkler nozzle (for the same water flow rate). On the contrary, the magnitude of the over-pressure peak is not sensitive to the water flow rate and the type of nozzle. Being influenced by the rate of warm up of the gas phase, this second peak depends mostly on the fire characteristics and not on those of the water system. In addition, the magnitude of the pressure peak when the water spray is activated is always larger than the magnitude of the peak at the water spray shut off. The pressure signal shows also a significant increase of the fluctuations during the period of water spraying. A comparison of the pressure fluctuations (standard deviation σ_P during a period of time) with and without water spraying is presented in Table 3. For all the tests, the period of water spraying gives larger pressure fluctuations (about 100 Pa of amplitude with water spraying in comparison with 20 Pa without water spraying). For the tests with sprinkler nozzles, the results indicate that the increase of water flow rate increases also the amplitude of the pressure fluctuations.

TABLE 3 Variation of the standard deviation of the pressure, σ_P, with and without water spraying and for the two nozzles

Test Name	PR2_FES_1	PR2_FES_2	PR2_FES_3	PR2_FES_4
Nozzle	Deluge	Deluge	Sprinkler	Sprinkler
Total flow rate (l/min)	110	110	110	157
σ_P (Pa) without spraying	23	28	19	22
σ_P (Pa) with spraying	131	107	61	115

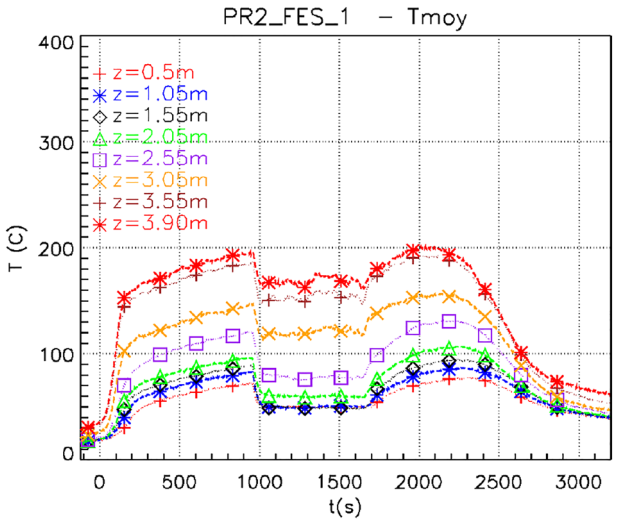

FIGURE 7 Time evolution of the mean gas temperature at several altitudes for the PR2_FES_1 test [Colour figure can be viewed at wileyonlinelibrary.com]

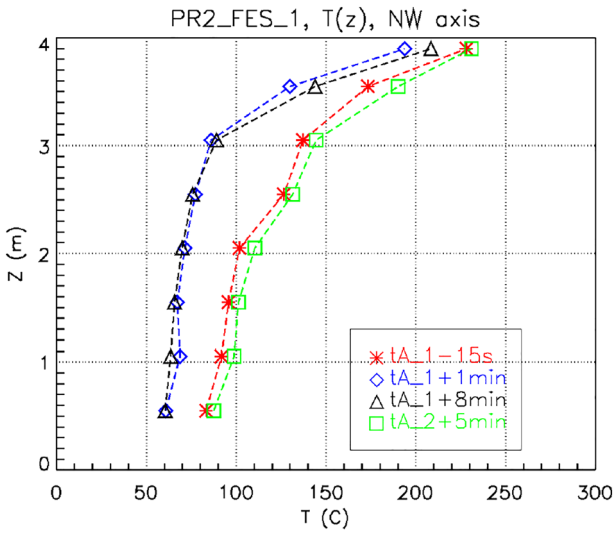

FIGURE 8 Vertical gas temperature profiles at four instant during the PR2_FES_1 fire test (tA_1 is the time of activation and tA_2 is the time of shut off) [Colour figure can be viewed at wileyonlinelibrary.com]

3.3 | Cooling of the gas phase

A third typical effect is the cooling of the gas phase by the water spraying. As an example, the time variation of the gas temperature at different height positions is presented in Figure 7 for the PR2_FES_1 test. During the period of water spraying ($[1000 : 1600]$ s), the gas temperature decreases significantly because of the heat transfers between the gas phase and the water droplets and restarts increasing when the water spray is stopped. The comparison of vertical temperature profiles taken at four instants (with and without water spraying) presented in Figure 8 illustrates also the process of smoke cooling. The vertical temperature profiles are shifted toward lower temperature for the times the water spraying is activated.

In order to quantify the net decrease of gas temperature, the difference between the temperature profile without water spraying (test PR2_FES_1 at $t = 500$ s) and with water spraying at the same time but with different water spraying conditions (deluge type at 110 l/min for PR2_FES_2 test, sprinkler type at 110 l/min for PR2_FES_3 test and deluge type at 157 l/min for PR2_FES_4 test) is presented in Figure 9. Although the application of water spraying system leads to gas cooling, it also leads to increase the MLR and therefore to an increase of the gas temperature. For all the tests, the net balance is hopefully a decrease of the gas temperature but with particular features. The net decrease is about 5 °C in average over the whole height with deluge type nozzles at 110 l/min. The change in nozzle type (deluge to sprinkler) increases this net temperature reduction to 15 °C. However, the increase of flow rate (from 110 l/min to 157 l/min) with sprinkler-type nozzles does not increase the temperature reduction. In that case, the raise of flow

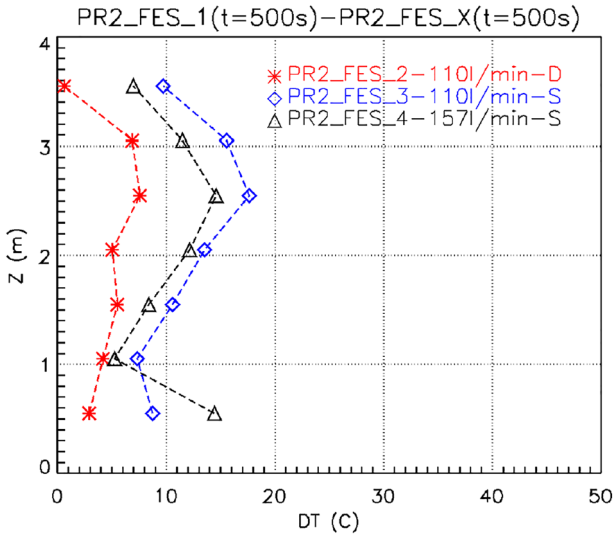

FIGURE 9 Difference of temperature between two profiles taken at the same time ($t = 500$ s) - Tmoy(z,test PR2_FES_1)-Tmoy(z,test x) for the three tests x= PR2_FES_2, PR2_FES_3, PR2_FES_4 [Colour figure can be viewed at wileyonlinelibrary.com]

rate increases much largely the MLR than the cooling process. Then, surprisingly, the net result is a better cooling with 110 l/min than with 157 l/min.

3.4 | Mixing of the gas phase

A last important effect of the water spraying is the mixing of the gas phase and the modification of the chemical stratification. This effect,

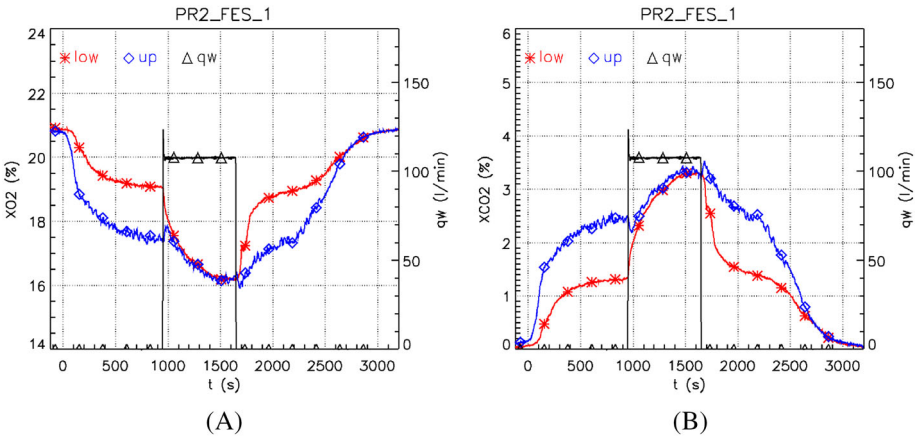

FIGURE 10 Time evolution of A, oxygen and B, carbon dioxide concentrations at two positions (lower and upper) for the PR2_FES_1 test [Colour figure can be viewed at wileyonlinelibrary.com]

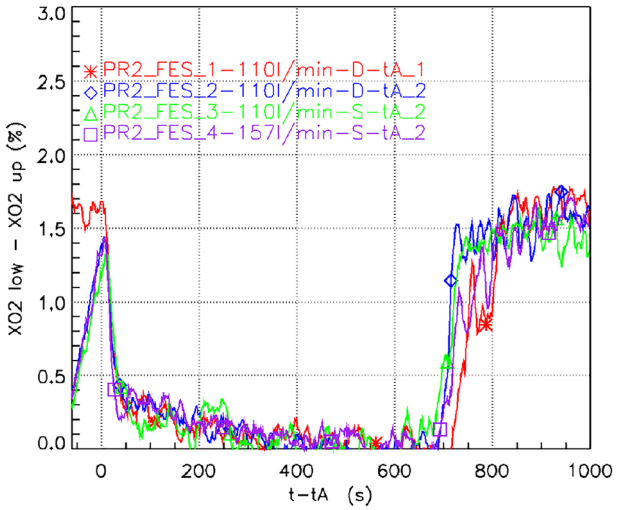

FIGURE 11 Time variation of the difference of oxygen concentrations between the upper and the lower parts of the compartment for all tests (t = 0 corresponds to the activation of water spraying) [Colour figure can be viewed at wileyonlinelibrary.com]

pointed out with gas propane fires,[3] is confirmed here with oil pool fires. This effect is illustrated in Figure 10 for the PR2_FES_1 test with deluge type nozzles and a water flow rate of 110 *l*/*min*. Without water spraying ($t < 1000$ s), the chemical stratification is characterized with smoke in the upper part of the compartment with a high concentration of carbon dioxide and a low concentration of oxygen. The lower part is less polluted and exhibits the highest level of oxygen concentration. Once the water spraying is activated, the concentrations measured at the two positions (upper part $z = 3.5$ m and in the lower part $z = 0.5$ m) are very rapidly equal indicating a strong homogenization of the gas by the spraying process.

The effect of the nozzle type and water flow rate on the chemical homogenization is showed in Figure 11. As soon as the water spraying is activated, the difference of concentrations between the upper and lower parts of the compartment drops down rapidly. For the oxygen species, there is no noticeable influence of the water flow rate and the nozzle type. The difference of concentration tends toward zero with the same behaviour.

These four large-scale fire experiments enable to collect some interesting features about the evolution of the MLR of a pool fire interacting with a water spray system and the four particular associated phenomena. By focusing on one fire experiment (namely PR2_FES_1) with the CFD CALIF^{3}S/ISIS software, the next section allows quantifying its ability to properly predict the effect of a water spray system on a mechanically ventilated compartment fire as well as the behaviour of some relevant physical quantities, namely the thermodynamic pressure, the thermal field, and the species concentration within the room along with the flow rates in the mechanical ventilation.

4 | CFD CALCULATION WITH CALIF^{3}S/ISIS

The CALIF^{3}S/ISIS* software, developed by IRSN, is a computational tool based on low-Mach number approximation dedicated to the simulation of fires in mechanically ventilated compartments. For the present study, a mixed formulation, Eulerian for the continuous phase and lagrangian for the discrete phase, is used to model the effect of a water aspersion through a thermal stratification in a mechanically ventilated compartment.

4.1 | Physical modelling

The balance equations[16,17] are written for a weakly compressible flow by using a low-Mach-number approach. In this case, the total pressure P_t is split into three contributions as follows:

$$P_t = P_{\text{th}} + p + \rho_0 g z, \tag{1}$$

where P_{th}, p, and $\rho_0 g z$ stand, respectively, for the thermodynamic, dynamic, and hydrostatic pressures. ρ_0 and g represent, respectively, the ambient density and the gravitational acceleration. P_{th} is constant in space, p depends on both space and time, and the hydrostatic part $\rho_0 g z$ varies only with the height z. As a turbulent flow is characterized by fluctuations of all local quantities, a Favre-averaging process is employed to describe the mean scalar and vector fields (eg, velocity and temperature). This averaged process requires closure rules dealt with a turbulence model.[18] The Reynolds-stress tensor and turbulent scalar fluxes are modelled using the eddy viscosity hypothesis and

*The CALIF^{3}S/ISIS software can be freely downloaded from the following website: https://gforge.irsn.fr/gf/project/isis/.

the first-order $k-\epsilon$ model with two balance equations. Standard wall functions are used to take into account the boundary layers as the two-equation closure model is no more valid near the walls where viscous effects are predominant. Turbulent combustion is based on the infinitely fast chemistry conserved scalar approach using the mixture fraction and the fuel mass fraction. The mean reaction rate, controlled by the turbulent flow mixing, is determined by the eddy dissipation combustion (EDC) model.[19] A one-step irreversible combustion reaction for the fuel is considered and involves oxygen and products in the presence of a neutral gas. Among the different approaches available in CALIF^{3}S/ISIS to model the soot production and transport, the simplest approach is to consider a coefficient (called soot conversion factor, ν_s) in the single one-step reaction.[20] The radiative transfers are dealt with the finite volume method[21] assuming a gray and nonscattering medium. The gas absorption coefficient of the mixture used the total emissivity approach of the weighted sum of gray gases model (WSGGM), and the soot absorption coefficient is related to the soot volume fraction according to the Mie theory. The wall conduction is taken into account through the 1*D* Fourier's equation and the convective flux is given by standard laws based on laminar and turbulent Prandtl numbers.[22]

The reader can refer to appendix A of ISIS 5.0.0.[16] for a detailed presentation of the governing balance equations solved by CALIF^{3}S/ISIS software, ie, the Navier-Stokes equations and scalar equations for turbulence, chemistry, enthalpy, and radiative transfer.

Concerning the boundary conditions, the experimental MLR is imposed at the fire source area, and the classical boundary conditions are applied on the walls.

4.2 | Mechanical ventilation modelling

As already mentioned, the thermodynamic pressure P_{th} is constant in space but a function of time.[23] Indeed, the thermodynamic pressure is expressed through the following overall mass balance equation:

$$\int_{\Omega} \frac{\partial}{\partial t}\left(\frac{P_{\text{th}} W}{\mathcal{R} T}\right) + \sum_i Q_i = 0, \tag{2}$$

where Q_i stands for the mass flow rate of the ventilation network at the branch i of the compartment, and the terms W, T, and $\mathcal{R}$ represent, respectively, the molecular weight of the air, the temperature, and the universal gas constant. To solve the $i+1$ unknowns, Equation 2 is supplemented with a momentum balance equation corresponding to a general Bernoulli equation for each branch of the ventilation network as follows:

$$\frac{L_i}{S_i}\frac{\partial Q_i}{\partial t} = P_t - P_t^{\text{ext,i}} - f, \tag{3}$$

where P_t and $P_t^{\text{ext,i}}$ represent, respectively, the total compartment pressure and the total external pressure at the extremity of the branch *i*. The head loss f is due to friction and is function of an aeraulic resistance R ($f = sgn(Q_i)RQ_i^2/\rho$). L_i and S_i represent, respectively, the length and surface of the branch *i*.

4.3 | Modelling of the dispersed phase

A dispersed liquid phase, composed of water droplets, is modelled in CALIF^{3}S/ISIS by a lagrangian technique. This phase exchanges mass, momentum, and heat with the surrounding fluid. The water phase is represented by a population of representative droplets (or samples), themselves composed by a fixed number of single identical droplets. Thanks to the calibration technique developped by Plumecocq et al,[24]the droplet size distribution (with an assumption of lognormal distribution) produced by the deluge spray nozzle during the PR2_FES_1 fire test was assessed previously by some experiments using a gas burner. For a volume flow-rate of 55 l.min^{-1}, the lognormal distribution of the nozzle is characterized by a mass median diameter of 5.6 10^{-4} m, a geometric standard deviation of 0.405 and an initial droplet velocity of 7 $m.s^{-1}$.

Each representative droplet is characterized by its position, its velocity, its temperature, and its mass. These quantities are determined by solving, for each representative droplet, the momentum, energy, and mass balance. In the momentum equation, the drag force using the Clift and Gauvin[25] drag coefficient is used. Concerning the heat transfer, a uniform temperature is assumed inside the droplet and the heat transfer considers the convective, radiative, and phase-change processes. The convective heat transfer obeys the classical Ranz-Marshall[26] correlation. The droplet evaporation follows the classical d^2 law provided by the evaporation-condensation theory from Spalding-Godsave.[27]

In addition, the interactions between the droplets and the carrier phase yield source terms in the balance equations for the carrier phase. In the mass balance equation, the mass source term is due to the evaporation process whereas in the momentum equation, the source term is the contribution of two phenomena. The first one is the interaction forces between the fluid and the droplets without any phase change (drag force) and the second one is the gas momentum flux due to the evaporation process. Finally, in the enthalpy equation, the source term represents the heat captured by the droplet for its heating and the heat released by the droplet into the fluid due to evaporation process. For more details about the formulation of the equations and the aforementioned interactions, the reader can refer to ISIS 5.0.0..[16]

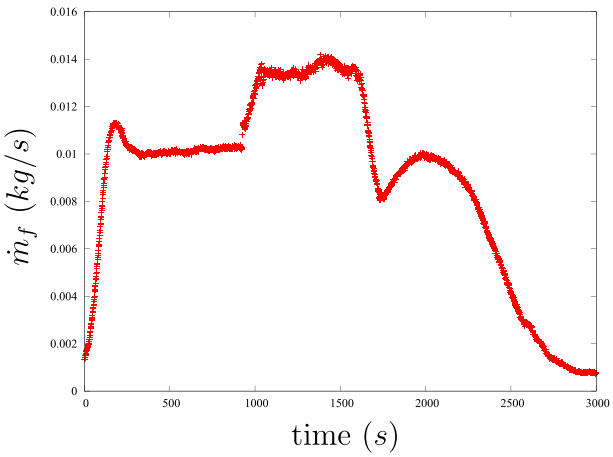

FIGURE 12 Time evolution of the fuel mass loss rate $\dot{m}_f$ of the PR2_FES_1 fire experiment [Colour figure can be viewed at wileyonlinelibrary.com]

5 | NUMERICAL RESULTS AND DISCUSSION

The PRISME FES experimental campaign has been achieved to investigate the performance of water spray systems to control the fire and the thermal stratification in a confined and mechanically ventilated enclosure. This campaign constitutes also a detailed database to assess the CFD tools on large-scale complex experiments including the fire and sprinkler events. Because of the numerous physical phenomena involved (eg, variable density flows, combustion, radiation, water spraying, interaction dispersed phase-continuous phase, and mechanical ventilation), the simulation of a FES fire experiment is challenging with a CFD software. This study focuses only on the PR2_FES_1 fire experiment for which the MLR $\dot{m}_f$ of the fuel is given in Figure 12.

In addition to the comparative analysis presented in Section 3.1 between the four large-scale tests, a more specific description of the MLR is presented below for the PR2_FES_1 fire experiment. First, from the ignition to $t \sim 200$ seconds, the fire growth rate of the fuel increases gradually up to a maximum value. Then, the fuel MLR stabilizes around a fixed value, $\dot{m}_f = 0.0105$ kg/s, and the regime of the fire can be assumed as steady. After around 12 minutes of steady state (at $t_a = 950$ seconds), the water spray system, composed of two deluge nozzles, is activated. We observe a sudden increase of the MLR, similar to the initial fire growth process and exhibiting the same time duration, approximately 120 seconds. Then, the fuel MLR stabilizes again to reach a new steady state. The fuel MLR $\dot{m}_f$ dramatically increases between the two steady states, by more than 25%, to reach the value of $\dot{m}_f = 0.013$ kg/s. This steady state continues until the end of the water spray at $t_e \sim 1645$ seconds. This enhancement of the MLR is, as already mentioned, an unexpected behaviour of the fire source considering that a water spray system is initially designed to prevent from fire risks and not to increase the fuel MLR. When the water system is shut down, a third transient phase is observed, with a sudden decrease of around 40% of the MLR down to $\dot{m}_f = 0.008$ kg/s. Then, the system tends to recover the first steady state but finally extinction occurs by lack of fuel. For the simulation of this study, the experimental MLR is imposed as boundary condition and is not predicted numerically in order to avoid the possible effect of nonmature pyrolysis model on the numerical results.

Simulations have been performed for three different meshes, namely M_1, M_2, and M_3. M_1 is a reference mesh with about 102 000 cells. The mesh M_2 is obtained from the mesh M_1 by increasing the number of cells in each direction by a factor $k_m \sim 1.35$. Again, the mesh M_3 is obtained from the mesh M_2 by increasing the number of cells in each direction by a factor $k_m \sim 1.35$ leading to about 620000 cells. The grid convergence is assessed on gas temperature at three points on the south-east thermocouple tree. The results presented in Figure 13 do not show differences greater than 40° C in the hot upper layer. This is considered as satisfactory for simulations of real large-scale fire scenario with water spray. In the following, the mesh M_2 is used for the simulation. Furthermore, we refer the reader to Suard, Lapuerta et al[28] and Suard, Koched et al[29] for the sensitivity analysis and the validation of the CALIF^{3}S-ISIS code.

We first focus on the thermodynamic pressure P_{th} representing a fundamental variable in the physics of confined and ventilated fires. The experimental plot is depicted in Figure 14. After the ignition, the transient fire growth leads to an increase of the temperature inside the compartment and consequently to an initial pressure increase up to a first pressure peak. The magnitude of this first overpressure peak is approximately 400 Pa. Then, the thermodynamic pressure P_{th} keeps constant on the first steady state before undergoing an underpressure peak when the water system is activated at t_a. This underpressure peak is characterized by, simultaneously, its significant magnitude and its briefness. Actually, the water activation leads to an underpressure peak more than twice than that of the overpressure peak observed at

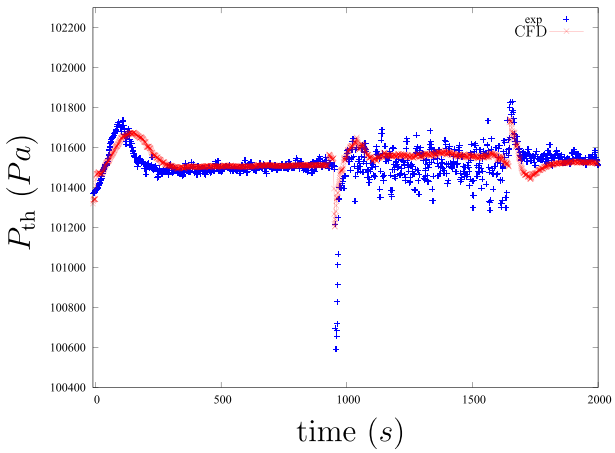

FIGURE 14 Time evolution of the thermodynamic pressure P_{th} inside the fire compartment [Colour figure can be viewed at wileyonlinelibrary.com]

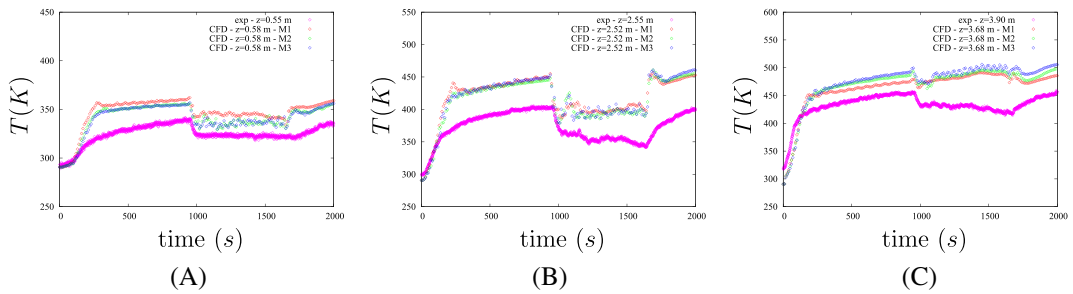

FIGURE 13 Time evolution of the temperature at different positions on the south-east thermocouple tree for three grid meshes M_1, M_2, and M_3 together with the experimental data [Colour figure can be viewed at wileyonlinelibrary.com]

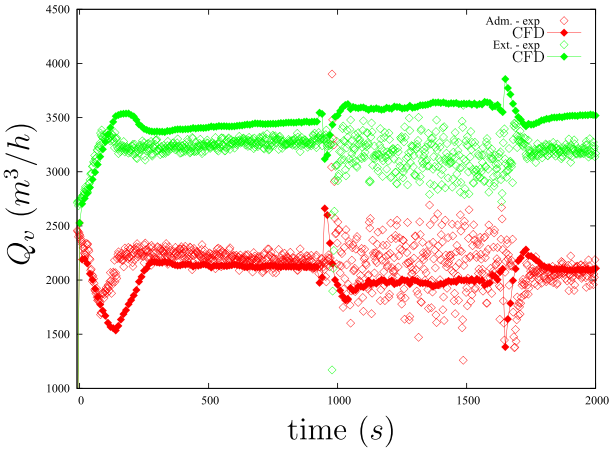

FIGURE 15 Time evolution of the ventilation volume flow rate Q_v in the admission and exhaust lines [Colour figure can be viewed at wileyonlinelibrary.com]

the ignition. Then, the experimental pressure fluctuates around $P_{th} \sim 101500$ Pa during the second steady state and a second overpressure peak is observed when the water spray system is turned off at t_e. The magnitude of this overpressure peak is around 300 Pa, ie, the third of the underpressure peak observed at t_a. For each peak of overpressure or underpressure (Figure 14), the time duration of the increase (decrease) is correctly estimated and in particular the sudden peak at the activation time t_a. The magnitudes of the peaks are properly estimated for the two overpressure peaks whereas the magnitude of the underpressure peak is underestimated.

As a consequence, the variation of thermodynamic pressure within the compartment has a significant effect on the mechanical ventilation regime, both in admission and exhaust. The time evolution of the experimental volume flow rate Q_v is depicted in Figure 15. As a

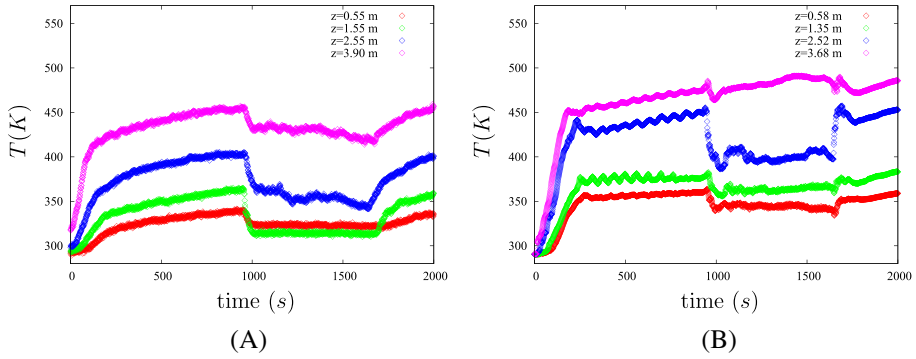

FIGURE 16 Time evolution of the temperature—A, from the experiment and B, from the simulation—at different positions on the south-east thermocouple tree [Colour figure can be viewed at wileyonlinelibrary.com]

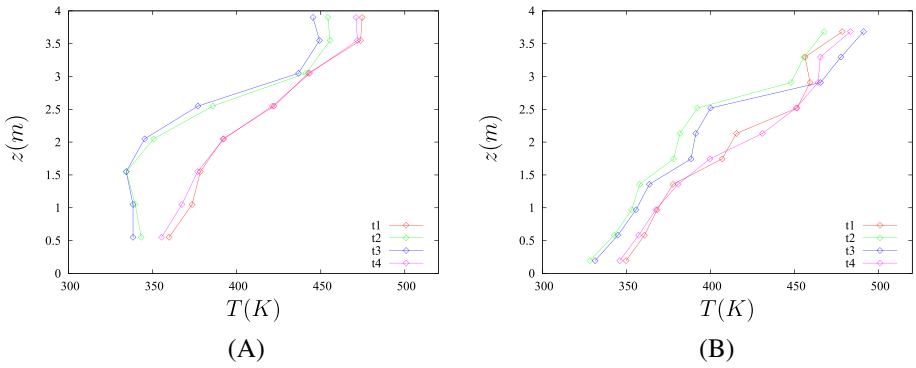

FIGURE 17 Vertical profiles of the temperature on the south-east thermocouple tree at four distinct times $t_1 = t_a - 15$ s, $t_2 = t_a + 1$ min, $t_3 = t_a + 8$ min, and $t_4 = t_e + 5$ min—A, from the experiment and B, from the simulation [Colour figure can be viewed at wileyonlinelibrary.com]

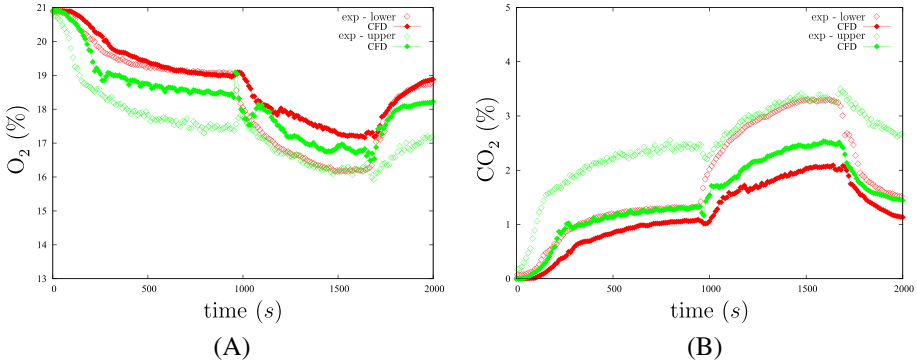

FIGURE 18 Time evolution of the A, oxygen B, carbon dioxide concentrations in the lower and upper positions [Colour figure can be viewed at wileyonlinelibrary.com]

response to the initial overpressure peak, the volume flow rate in the admission is temporarily reduced at the opposite of the exhaust where it is enhanced. Then, to the steady fire state corresponds a steady ventilation state both in admission and extraction. Furthermore, as a response to the underpressure peak related to the activation of the water spray system, the volume flow rate Q_v suddenly increases in the admission line whereas it decreases in the exhaust line. Of course, an opposite behaviour is observed when the water spray system is shut down. In Figure 15, the overall behaviour is satisfactorily reproduced with the CFD simulation both in admission and extraction ducts, especially the fairly good agreement observed in the magnitudes of the peaks at t_a and t_e.

It seems now of interest to characterize the thermal field within the enclosure during such an experiment. In Figure 16 is given the time evolution of temperature on the south-east thermocouple tree from the experiment and the simulation. After a sudden heating of the enclosure during the initial fire growth phase, the temperatures during the steady state adopt a different behaviour following the vertical position. Indeed, a slight increase of temperature is observed in the upper part of the enclosure whereas in the lower part, it remains nearly constant. Actually, the upper part continuously receives hot smoke, which slightly increases the thermal field despite the exhaust ventilation. The lower part is less affected and the thermal field keeps less unchanged. Once the water spray is activated, it is logically observed a sudden decrease of the thermal field, especially in the zones located at an height below the sprinkler positions and in the intermediate vertical altitudes. The gas cooling can attain 50 K at the maximum and 15 K in the regions far from the sprinklers.

Concerning the thermal stratification within the enclosure, Figure 17A represents the experimental vertical temperature profile on the south-east thermocouple tree at four representative times, t_1, t_2, t_3, and t_4, corresponding, respectively, to the first steady state (before the water spray activation), the beginning of the second steady state (during the aspersion), the end of the second steady state, and after the extinction of the water spray. From a usual temperature profile observed at the steady state (t_1) of a mechanically ventilated enclosure fire, the activation of the water spray (time t_2) cools the enclosure over its whole height and the stratification evolves from a progressively increasing thermal gradient with the altitude to the appearance of three distinct zones. This is confirmed with increasing the aspersion time (time t_3) where a quasi constant cool zone over $[0:2\,m]$ is observed then followed by a steep thermal gradient zone ($[2:3\,m]$) and a third hot layer ($[3:4\,m]$) . Once the water spray is stopped, the system recovers the thermal stratification before the water aspersion. The thermal profiles given by the simulation, depicted in Figure 17B, properly predict the gas cooling due to the aspersion but in a less pronounced way for the intermediate heights.

In addition to the temperature field within the enclosure, it is also of interest to focus on the evolution of the gas concentration within the enclosure. Concentrations of oxygen and carbon dioxide are depicted in Figure 18 for two vertical positions corresponding to the locations of the gas sensors, located in the lower and upper parts. The outstanding feature attributed to aspersion to mix the gases and to make almost homogeneous the O_2 and CO_2 concentrations in the upper part and in the lower part is also satisfactorily recovered by the simulation, although a maximum of absolute difference of 1% for these species between the experiment and the simulation can be considered as non negligible.

6 | CONCLUSION

The present contribution investigates the case of a confined and forced ventilated enclosure fire scenario and its interaction with a water spray system in the framework of the OECD PRISME2 project. We first examine the experimental fuel MLR for four operating conditions, taking into account the influence of the activation time of the water spray, the type of nozzle, and the water flow rate. All the tests are characterized by an initial fire growth period followed by a steady phase of combustion during which the activation of the water spray contributes to increase the MLR. When water spray is shut off, we observe a decay of the MLR and the extinction of the fire due to lack of fuel. The use of CALIF^{3}S/ISIS software on one specific scenario (PR2_FES_1), with the experimental MLR imposed as a boundary condition, compares satisfactorily with the experiment on typical variables of interest such as the thermodynamic pressure, the thermal field, and species concentrations within the compartment as well as flow rates in the mechanical ventilation. Four typical mechanisms are identified. First, the cooling of the gas phase is observed when the water spray system is activated accompanied by a gas mixing phase leading to a homogenization within the enclosure. The third effect is the significant increase of the MLR (and consequently of the heat release rate) and the last noteworthy effect is the occurence of opposite gas pressure peaks when the water spray system is activated and shut off.

ORCID

Samuel Vaux https://orcid.org/0000-0002-6544-9701
Hugues Prétrel https://orcid.org/0000-0003-3044-5695

REFERENCES

1. Myers TM, Marshall AW. A description of the initial fire sprinkler spray. *Fire Saf J*. 2016;84:1-7.
2. Pretrel H, Le Saux W, Audouin L. Pressure variations induced by a pool fire in a well-confined and force-ventilated compartment. *Fire Saf J*. 2012;52:11-24.
3. Pretrel H. Interactions between water sprays and smoke filling in case of a fire event in a closed and mechanically ventilated compartment. *Fire Saf J*. 2017;91:336-346.
4. Li KY, Huo R, Ji J, Ren B. Experimental investigation on drag effect of sprinkler spray to adjacent horizontal natural smoke venting. *J Hazard Mater*. 2009;174:512-521.
5. Li KY, Spearpoint J. Simplified calculation method for determining smoke downdrag due to a sprinkler spray. *Fire Technol*. 2011;47:781-800.
6. Li KY, Spearpoint J. Evaluation of simplified calculation methods for determining heat transfer between a smoke flow and a sprinkler spray. *J Fire Sci*. 2012;30:92-109.
7. Li KY, Hu LH, Huo R, Li YZ, Chen ZB, Li SC, Sun XQ. A mathematical model on interaction of smoke layer with sprinkler spray. *Fire Saf J*. 2009;44:96-105.

8. Tang Z, Vierendeels J, Fang Z, Merci B. Description and application of an analytical model to quantify downward smoke displacement caused by a water spray. *Fire Saf J*. 2013;55:50-60.
9. Chung KC, Tung HS. A simplified model for smoke filling time calculation with sprinkler effects. *J Fire Sci*. 2005;23:279-300.
10. Crocker JP, Rangwala AS, Dembsey NA, Leblanc DJ. Investigation of sprinkler sprays on fire induced doorway flows. *Fire Technol*. 2010;46:347-362.
11. Li Y, Chow W. Study of water droplet behavior in hot air layer in fire extinguishment. *Fire Technol*. 2008;44:351-381.
12. Yao B, Chow W. Smoke venting effect when discharging a solid cone water spray. *J Appl Fire Sci*. 2010;20:201-209.
13. Pretrel H, Querre P. Repeatability assessment of large-scale fire experiment involving water spray system in a forced ventilated compartment. *Fire and Materials*. 2018:1-12. https://doi.org.10.1002/fam.2679
14. Mawhinney JR, Dlugogorski BZ, Kim AK. A closer look at the fire extinguishing properties of water mist. In: Fire safety science, Proceedings of the Fourth International Symposium, 13-17 July 1994; 1994; Ottawa, Ontario, Canada:47-58.
15. Richard J, Garo JP, Souil JM, Vantelon JP, Knorre VG. Chemical and physical effects of water vapor addition on diffusion flames. *Fire Safety Journal*. 2003;38:569-587.
16. ISIS 5.0.0. Physical Modelling. Institut de Radioprotection et de Sûreté Nucléaire, https://gforge.irsn.fr/gf/project/isis/.
17. Suard S, Forestier M, Vaux S. Toward predictive simulations of pool fires in mechanically ventilated compartments. *Fire Saf J*. 2013;61:54-64.
18. Novozhilov V. Computational fluid dynamics modeling of compartment fires. *Prog Energy Combust Sci*. 2001;27(6):611-666.
19. Magnussen BF, Hjertager BH. On mathematical modeling of turbulent combustion with special emphasis on soot formation and combustion. In: Symposium International on Combustion 16; 1976; Pittsburgh:719-729.
20. Novozhilov V, Koseki H. CFD prediction of pool fire burning rates and flame feedback. *Combust Sci Technol*. 2004;176:1283-1307.
21. Chai JC, Lee HS, Patankar SV. Finite volume method for radiation heat transfer. *J Thermophys Heat Transf*. 1994;8:419-425.
22. Cox G.. *Combustion fundamentals of fire*. London, San Diego: Academic Press; 1995.
23. Suard S, Lapuerta C, Babik F, Rigollet R. Verification and validation of a CFD model for simulations of large-scale compartment fires. *Nucl Eng Des*. 2011;241(9):3645-3657.
24. Plumecocq W, Audouin L, Joret JP, Pretrel H. Numerical method for determining water droplets size distributions of spray nozzles using a two-zone model. *Nucl Eng Des*. 2017;324:67-77.
25. Clift R, Gauvin WH. Motion of entrained particles in gas streams. *Can J Chem Eng*. 1971;49(4):439-448.
26. Ranz WE, Marshall WR. Evaporation from drops. *Chem Eng Prog*. 1952;48:141-146.
27. Spalding DB. The combustion of liquid fuels. Symposium (International) on Combustion. *Fourth Symp (Int) on Combustion*. 1953;4(1):847-864.
28. Suard S, Lapuerta C, Kaiss A, Porterie B. Sensitivity analysis of a fire field model in the case of a large-scale compartment fire scenario. *Num Heat Trans, Part A*. 2013;63:879-905.
29. Suard S, Koched A, Pretrel H, Audouin L. Numerical simulations of fire-induced doorway flows in a small scale enclosure. *Int J Heat Mass Trans*. 2015;81:578-590.

How to cite this article: Vaux S, Prétrel H, Audouin L. Experimental and numerical study of water spray system for a fire event in a confined and mechanically ventilated compartment. *Fire and Materials*. 2019;43:579–590. https://doi.org/10.1002/fam.2719